Directional Antenna based Spatial and Energy Efficient Semi-Distributed Spectrum Sensing in Cognitive Internet-of-Things Networks

Chunghyun Lee, Junsuk Oh, Woongsoo Na, Jongha Yoon, Wonjong Noh and Sungrae Cho

C. Lee, J. Oh, and S. Cho are with the School of Software, ChungAng University, Seoul, Republic of Korea, e-mail: chlee@uclab.re.kr; jsoh@uclab.re.kr; srcho@cau.ac.kr.

J. Yoon is with Air and Missile Defense Team in Hanwha Systems, Seongnam, Republic of Korea, e-mail: jhyoon@hanwha.com

W. Na is with Division of Computer Science and Engineering, Kongju National University, Cheonan, Republic of Korea, e-mail: wsna@kongju.ac.kr.

W. Noh is with the School of Software, Hallym University, Chuncheon, Republic of Korea, e-mail: wonjong.noh@hallym.ac.kr.

Abstract

Recently, cognitive networks and mmWave-based massive antenna transmission are becoming promising approaches for high performance in dense, complicated 6G networks. However, accurate and efficient spectrum sensing that can provide primary user and secondary user (SU) with satisfactory performance is still difficult. In this paper, we propose a new semi-distributed and cooperative passive spectrum sensing method for directional antenna based cognitive radio networks, which can be considered as a key technology of industrial-internet-of-things systems. It finds optimal directional sensing-beams and spectrum detection energy threshold to maximizes a system utilization that consists of accurate spectrum sensing probability and spatial efficiency. To find the optimal controls in a semi-distributed manner, we employ a modified elimination method and a low-complex coordination algorithm among localized user groups with proof of concavity. The simulation results reveal that the proposed control provides enhanced spectrum sensing in terms of sensing accuracy, spatial efficiency, and energy consumption compared to legacy omnidirectional antenna-based sensing approach and directional antenna-based fully distributed sensing approach. In fact, the performance gain becomes larger as the number of SUs increases. We also confirm that the proposed scheme achieves a near-optimal performance within around 5% of a directional antenna-based centralized sensing approach.

Keywords: Wireless network, Cognitive radio, Distributed computing, Internet of Things

1. Introduction

In future communication systems, the availability of a communication resource is expected to become increasingly challenging issue because of the extensive growth in mobile traffic demands. To address the problem, first, a new hierarchical communication system, cognitive radio networks (CRNs), consists of primary users (PUs) and secondary users (SUs) is emerging and attracting growing attention for deployment [1]. Second, directional-transmission communication systems based on massive antenna and mmWave-frequency resources are being actively exploited. In this work, we consider a system that combines the directional antenna technology and CRNs, referred to as a distributed CRNs (D-CRNs). This emerging technique has many advantages over legacy radio systems. First, new various device-to-device (D2D) and vehicle-to-everything (V2X) communication systems can be implemented efficiently without installing additional infrastructure or with minimal infrastructure. Second, exponentially increasing various internet-of-things (IoT) equipment can be deployed without incurring seriously interfering with neighboring users

In general, in cognitive-based networks, SUs perform regularly or occasionally perform spectrum sensing to verify whether the spectrum licensed to PUs is vacant. And if so, SUs perform spectrum sensing to verify whether the channel quality is acceptable. The networks are permitted to use vacant or high quality licensed spectrum while limiting interference with PUs. However, unless the spectrum is vacant or of high quality, SUs should decrease their transmission powers to reduce their interference levels or switch to a new vacant channel. Moreover, in directional antenna-based networks, accurate energy-efficient beam usage is critical to system performance. Therefore, in this work, we focus on spatial and energy-efficient directional spectrum sensing in D-CRNs.

1.1. Related Work

Cooperative spectrum sensing schemes can be classified into two categories depending how SUs share their sensing information in the network [2]: *centralized* and *distributed*.

1.1.1. Centralized Cooperative Spectrum Sensing

Centralized CRN (C-CRN) schemes [**?** 3, 4, 5] exploit a coordinator called a fusion center (FC) that gathers sensing information from SUs, computes the sensing schedule for the SUs, and disseminates parameters to the SUs. Na *et al.* [**?**] proposed a centralized cooperative directional sensing scheme in CRNs.

Using a modified gradient descent method, the scheme minimized the sensing overhead by optimizing the sensing period, power, and beams of each secondary node. Simulation results demonstrate that our directional spectrum sensing technique is well suited for the existing cognitive radio environment. Wan *et al*. [3] proposed a cooperative spectrum sensing scheme for IoT network. In the proposed scheme, the spectrum sensing technique is further devised to the spatial dimension. This technique ias differentiated from the above study by considering spatial correlation. The information derived from spatial correlation is related to the probability of detection and spectrum utilization to enhance the energy efficiency. Paul *et al*. [4] proposed a spectrum sensing scheme for vehicular networks based on decision fusion techniques using renewal theory model. The proposed techniques can solve the frequent interference and hidden PU problems in vehicular networks. Wu *et al*. [5] proposed a cooperative sensing technique based on maximum a posterior-Markov random field (MAP-MRF) framework which focuses on the individual spectrum coverage of the SU. Spectrum state information from each SU is exchanged and aggregated with its neighbors using belief-propagation (BP) algorithm. Generally, the performance of the cooperative spectrum sensing approaches is satisfactory. However, these C-CRN schemes typically derive significant control overhead and energy consumption for collecting sensing information and beam scheduling decisions. Moreover, the arrangement problem of PUs such as drones or satellites is still challenging in C-CRNs. [6]. Above all, the problem of inactivating the sensing function when the FC is stopped and a security problem that makes the FC vulnerable in case of malicious behavior urgently need to be addressed [7]. To address these issues, various distributed spectrum sensing schemes in CRNs have begun to be studied.

Table 1: Notations description

Notation	Description
N, M	The number of SU and beam
$K, \hat{K}$	The number of subchannel and LBZ
$\mathrm{SU}_{i,j}$	The jth beam of ith SU
R	The coverage of an SU
$L^{i}_{j,n}(x)$	A linear equation
$R_{i,j}(x)$	A circular equation
$P^{i,j}_{j,n}$	An intersection point
$C_i(x_i, y_i)$	The centroid of ith SU
θ	The beam-sector angle
$\Upsilon_{i,j}$	The measured SNR
$\lambda_{i,j}$	The detection margin (threshold)
Λ	The set of λ
P_{FA}	The false-alarm probability
P_{CD}	The correct-detection probability
$\Phi_{i,j}$	The probability of accurate-sensing
W	The bandwidth in system model
T_s, T_d	The time of sensing and transmission
u	The time-bandwidth product
$\mathrm{E}^{U}_{d}(x)$, $\mathrm{E}^{L}_{d}(x)$	Upper and lower equation
$[\mathrm{p}_d, \mathrm{q}_d]$	An overlapped subinterval region
i_d	The d-th subinterval information
$\mathrm{I}_{i,j}(m, n)$	The set of i_d
$\Psi_{i,j}$	The overlapping beam coverage ratio
$A_{i,j}$	The area of $\mathrm{SU}_{i,j}$
$s_{i,j}$	The beam decision binary indicator
$\mathcal{S}$	The set of $s_{i,j}$
α, β	The weight factor for normalization

1.1.2. Distributed Cooperative Spectrum Sensing

In D-CRNs, unlike C-CRNs, SUs share sensing information without FC and determine their sensing schedules independently. Distributed methods in CRNs sense the spectrum better due to their fast adaptation to network changes. They also consume less power, which is critical in CRNs. Most previous spectrum sensing techniques use omnidirectional antennas. However, the use of directional antennas for spectrum sensing is a promising technique that can realize fine-grained sensing for a PU with a longer sensing range. Various distributed spectrum sensing schemes for D-CRNs[8, 9, 10, 11] have been proposed. Gazestani *et al*. [8] proposed a diffusion-based distributed sensing scheme for CRNs, which improves the robustness of the spectrum sensing method against link failure and network topology changes. The convergence rate and mean square error under a link failure assumption were analyzed in practical realistic scenario. The method achieved a better convergence rate and level of accuracy then conventional distributed methods. Smith *et al*. [9] proposed spectrum sensing in a CRN with arbitrary numbers of PUs and SUs. Based on the sphericity test, it analyzed the centralized spectrum sensing where all the data available at the SUs are combined for the signal detection of PUs. It found accurate approximations for the false-alarm and detection probabilities. Gu *et al*. [10] proposed a distributed available spectrum sensing and allocation algorithm called a rendezvous algorithm. It assumed that the users have different sensing capabilities due to hardware differences. The proposed heterogeneous sensing algorithm has enhanced time efficiency, but the algorithm does not consider energy efficiency.

1.2. Motivation, Contribution, and Organization

Table 2 summarizes key features of the proposed scheme and key differences from existing scheme. The major contributions of this research can be summarized as follows:

- We formulated a semi-distributed cooperative spectrum sensing problem in CRNs to maximize the probability of accurate spectrum sensing and overlapping beam coverage ratio (OBCR), which is related to spatial and energy efficiency. The centralized cooperative spectrum sensing scheme relies extensively on the FC, which can have system stability and scalability issues. In contrast, distributed cooperative spectrum sensing problem has greater complexity and poorer performance than centralized cooperative spectrum sensing. Therefore, we transform the centralized spectrum sensing problem into a distributed spectrum sensing problem.

Table 2: Summary of key features and differences (spectrum sensing techniques)

Reference	Centralized	Distributed	Sensing Probability	Energy Efficiency	Spatial Correlation
[**?**]	✓	×	✓	✓	×
[3]	✓	×	✓	✓	✓
[4]	✓	✓	✓	×	×
[5]	✓	✓	✓	✓	×
[8]	×	✓	✓	×	×
[9]	✓	✓	✓	×	×
[10]	×	✓	×	×	×
[12]	×	✓	✓	×	×
[11]	×	✓	×	✓	×
Proposed	✓	✓	✓	✓	✓

- To solve the centralized spectrum sensing problem in a distributed manner, we initially form a cooperative localized coalition called localized broadcast zones (LBZs). Then, we propose a semi-distributed and cooperative spectrum sensing scheme that can be employed within each LBZ. In addition, we proposed *a low-complexity coordination mechanism* between LBZ leaders to ensure efficient spectrum sensing.
- Through extensive simulations, we confirmed that the proposed control provides better sensing accuracy, spatial efficiency, and energy consumption than traditional omnidirectional antenna-based sensing and directional antenna-based fully distributed sensing approaches. The performance gain increased with the number of SUs. More importantly, the proposed scheme achieved near-optimal performance within approximately 5% of that of a directional antenna-based centralized cooperative spectrum sensing approach.

The remainder of this paper is organized as follows. The system model and problem formulation are presented in Sections 2 and 3, respectively. The proposed semi-distributed optimization solution is presented in Section 4. The performance evaluation and conclusions are described in Sections 5 and 6, respectively. In addition, the notation used in this paper is summarized in Table 1.

2. System Models

In this section, we describe the system model considered in this paper.

2.1. Primary User

In this work, we assume that PU is equipped an omnidirectional antenna, as depicted in Fig. 1a, operated in a slotted fashion. Furthermore, PUs periodically broadcast pilot signals, which are cyclostationary, such as in digital video broadcasting-terrestrial (DVB-T) [13] in IEEE 802.22, a standard for a wireless regional area network (WRAN) using the white space band of the television frequency band [14].

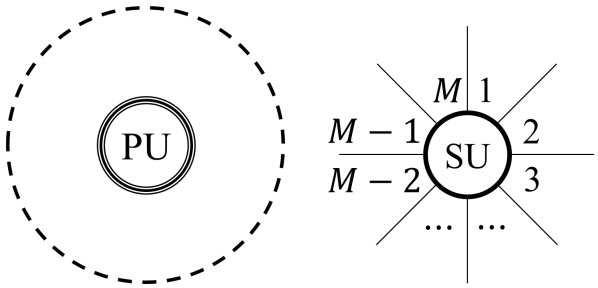

(a) Primary User Model (b) Secondary User Model

Figure 1: Proposed antenna models of primary user (PU) and secondary user (SU). PUs are equipped an omnidirectional antenna while SUs are equipped with directional antennas.

2.2. Secondary User

In this system, there are N SUs and the ith SU is denoted as SU_i. Each SU is equipped with a directional antenna, and each directional antenna has M beam directions, as in Fig. 1b. It is assumed that SUs are static, and SUs know information about neighboring nodes, such as their number, locations, and beam angle. This information can be obtained from initial setup process, such as exchange of a "Hello" message in the practical standard system.

2.3. Antenna and Beam Model

The directional antenna consists of M directional beams and can be switched between transmitting and receiving modes with an antenna controller. The switching is implemented within the antenna controller using very fast analog complementary metal-oxide-semiconductor (CMOS) multiplexers/demultiplexers, which have a fast transition time of fewer than $217ns$ and less than signal propagation delay [15]. Here, we assume that the side lobe of each beam is much smaller than the main lobe. That is, the side lobe is negligible, and each beam patterns can be treated as ideally non-overlapping. Each beam has the same angle θ, namely, $\theta = \frac{2\pi}{M}$.

2.4. Channels

In this system, the PU licensed band is divided into K channels, and SUs can opportunistically use the K data channels to

transmit or receive their data. To exploit the PU's data channels, SUs perform channel sensing for K channels to identify any spectrum hole. We assume that SUs use a dedicated control channel to share information their obtained with each other [16, 17]. As a communication protocol for the control channel among SUs, we employ LoRa, a type of a low-power wide-area network (LPWAN) technology that operates on low power and has a wide communication range and multi-sensing capability [18].

2.5. Localized Broadcast Zone Model without Fusion Center

Algorithm 1 Localized Broadcast Zone Grouping Scheme

i, j : index of SU
k : index of LBZ
$\hat{K}$: number of LBZs
Step 1. ***Update the local information between SUs***
All SUs broadcast their local information.
Step 2. ***Formulate LBZ according to definition*** (1)
$k \leftarrow 1$
while even one SU does not belong to any LBZ **do**
  for $i := 1$ to N **do**
    if SU_i is not contained any LBZ **then**
      $\text{LBZ}_k = LBZ_k \cup SU_i$
      for $j := i + 1$ to N **do**
        if SU_j is not contained any LBZ **then**
          if $D(i, j) < R$ **then**
            $\text{LBZ}_k = LBZ_k \cup SU_j$
          end if
        end if
      end for
    end if
  end for
  $k \leftarrow k + 1$
end while
$\hat{K} \leftarrow k$
Step 3. ***Select the LBZ leader among the SUs***
$a_{min} \leftarrow \infty$
for $k := 1$ to $\hat{K}$ **do**
  $x^k = \frac{\sum_{i=1}^{|LBZ|} x_i}{\hat{K}}$
  $y^k = \frac{\sum_{i=1}^{|LBZ|} y_i}{\hat{K}}$
  for $i := 1$ to $|LBZ_k|$ **do**
    $a = \sqrt{(x_i - x^k)^2 + (y_i - y^k)^2}$
    if $a_{min} \geq a$ **then**
      $a_{min} \leftarrow a$
      LBZ leader is updated to SU_i.
    end if
  end for
end for

In this work, unlike a global FC, as in Fig. 2a, we use a local clustering-based semi-distributed model, as in Fig. 2b. Each local cluster is referred to as an LBZ [19]. The LBZ is defined as follows:

$$\text{LBZ}_k = \{\text{SU}_i | D(i, j) < R, \ \forall i, j \in \text{LBZ}_k\}, \qquad (1)$$

where k is the index of LBZ and $D(i, j)$ is a distance between SU_i and SU_j. In each LBZ_k, there is an LBZ leader, and all the SUs in the same LBZ_k transmit their sensing information to the LBZ leader using multi-hop routing algorithm [20]. Algorithm 1 shows how the LBZs are formed and their local leaders determined.

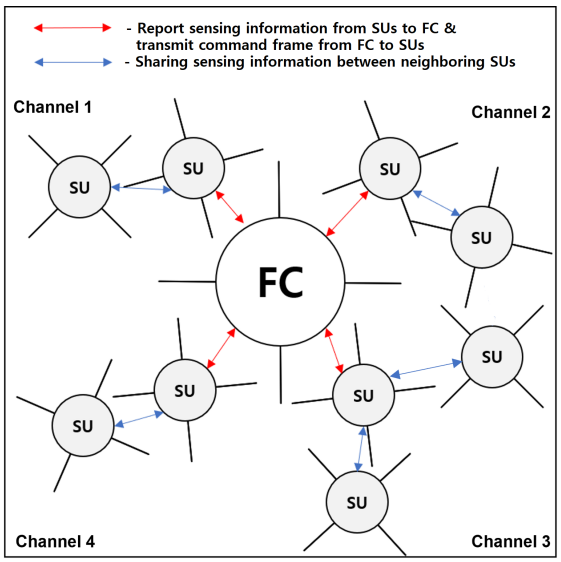

(a) Centralized system model.

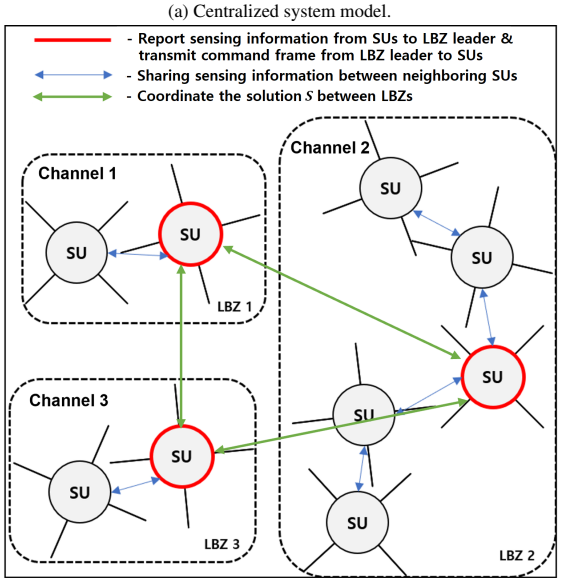

(b) Semi-distributed system model.

Figure 2: System models: the centralized model (a) and proposed semi-distributed model (b).

2.6. Licensed Spectrum Sensing Method

One of the most important functions in cognitive radio is to efficiently detect whether SUs have available spectrum to use without interfering with PUs. There are many approaches to spectrum sensing methods: energy detection, second-order statistics, statistical pattern recognition, feature template, matched filter and cyclostationarity detection methods [21], [22]. Many of these systems in recent studies have used the energy-detection

method [14],[23] owing to its minimal hardware cost [**?**]. However, it requires some SU quiet periods to distinguish the PU signals and other noise. In addition, to ensure a quiet period in a distributed environment, all SUs must be synchronized, which is a very difficult task without an FC. Therefore, in this work, we use the energy-detection sensing technique with unsynchronized SU quiet periods, with the help of PU cyclostationary pilot patterns, which are usually open to the public [13].

3. Problem Formulation

In this section, we elaborate on the proposed optimization problem. We first explain accurate-sensing probability and overlapping beam coverage ratio (OBCR), which are major factors for the proposed efficient spectrum sensing, and then present our problem formulation.

3.1. Accurate-sensing Probability

The accurate-sensing probability can be evaluated based on two hypotheses, H_0 and H_1:

H_0 : PUs are absent (a subchannel is not being used),

H_1 : PUs are present (a subchannel is being used).

Under H_0 and H_1, the false-alarm probability $P_{FA}(\cdot)$ and correct-detection probability $P_{CD}(\cdot)$ can be evaluated as follows:

$$P_{FA}(\lambda_{i,j}) = P\left(\mathrm{SU}_{i,j} \text{ detects at least one PU under } \lambda_{i,j} | H_0\right),$$

$$P_{CD}(\lambda_{i,j}) = P\left(\mathrm{SU}_{i,j} \text{ detects at least one PU under } \lambda_{i,j} | H_1\right),$$

where $\lambda_{i,j}$ represents the energy-detection threshold for PU signals. Based on [**?**],[24], the probabilities $P_{FA}(\cdot)$ and $P_{CD}(\cdot)$ can be expressed as

$$P_{FA}(\lambda_{i,j}) = \frac{\Gamma\left(u, \frac{\lambda_{i,j}}{2}\right)}{\Gamma(u)}, \tag{2}$$

$$P_{CD}(\lambda_{i,j}) = Q_1\left(\sqrt{2\Upsilon_{i,j}}, \sqrt{\lambda_{i,j}}\right), \tag{3}$$

where $\Gamma(\cdot)$ denotes the gamma function, $\Gamma(\cdot,\cdot)$ represents the upper incomplete gamma function, and $Q_1(\cdot)$ indicates the generalized Marcum Q function with the first-order-modified Bessel function [25]. In (2), u denotes a sensing time-bandwidth product and it is usually approximated to 1 [**?**]. In (3), $\Upsilon_{i,j}$ represents the measured signal-to-noise ratio (SNR) of the PU signal. For sensing, the SU determines the presence of PUs based on energy detection with a constant sensing period T_s Then, the accurate-sensing probability $\Phi_{i,j}(\lambda_{i,j})$ can be obtained as follows:

$$\begin{aligned}
&\Phi_{i,j}(\lambda_{i,j}) \\
&= \left(1 - P_{FA}\left(\lambda_{i,j}\right)\right) P(H_0) + P_{CD}(\lambda_{i,j}) P(H_1), \\
&= \left(1 - \frac{\Gamma(1, \frac{\lambda_{i,j}}{2})}{\Gamma(1)}\right) P(H_0) + Q_1\left(\sqrt{2\Upsilon_{i,j}}, \sqrt{\lambda_{i,j}}\right) P(H_1),
\end{aligned} \tag{4}$$

where $P(H_0)$ and $P(H_1)$ denote the probabilities of hypotheses H_0 and H_1, respectively, during the sensing period and satisfy $P(H_0) + P(H_1) = 1$.

3.2. Overlapping Beam Coverage Ratio (OBCR)

When a sensing beam that significantly overlaps a neighboring beam area is turned on, many sensing beams may not need to perform beam sensing, allowing that much energy to be conserved. That is, we need to estimate how much the area overlaps the area of the other beam when one beam is turned on. We define this overlapping degree as OBCR.

To this end, we first determine overlapping points among all the beam sectors of the SUs in the same LBZ. The information on the overlapping points between a particular $\mathrm{SU}_{i,j}$ and another beam $\mathrm{SU}_{m,n}$ in the same LBZ is denoted as $I_{i,j}(m,n)$,

$$I_{i,j}(m,n) = \left\{ i_d | i_d = (p_d, q_d, E_d^U, E_d^L) \right\}, \tag{5}$$

where i_d denotes the d-th overlapping subinterval region $[p_d, q_d]$ that is upper- and lower-bounded by E_m^U and E_m^L, respectively. For the example in Fig. 3, the information on the overlapping points for SU_{11} can be expressed as follows:

$$\begin{aligned}
I_{1,1}(2,2) &= \{(x_{1,1}^{'}, x_{2,1}, E_{13}, E_{23}), (x_{2,1}, x_{1,2}^{'}, E_{21}, E_{23})\}, \\
I_{1,1}(2,3) &= \{(x_{2,1}, x_{1,2}^{'}, E_{32}, E_{33}), (x_{1,2}^{'}, x_{1,3}^{'}, E_{32}, E_{13}), \\
&\qquad (x_{1,3}^{'}, x_{1,3}, E_{12}, E_{33})\}, \\
I_{1,1}(3,4) &= \{(x_{1,4}^{'}, x_{1,5}^{'}, E_{43}, E_{12}), (x_{1,5}^{'}, x_{1,3}, E_{43}, E_{13})\}.
\end{aligned}$$

After finding the information about the overlapping subintervals, the OBCR $\Psi_{i,j}$ for each beam sector can be calculated as follows:

$$\Psi_{i,j} = \frac{1}{A_{i,j}} \sum_{m=1}^{|LBZ_k|} \sum_{n=1}^{M} \sum_{d=1}^{|I_{i,j}(m,n)|} \int_{p_d}^{q_d} \left[E_d^U(x) - E_d^L(x) \right] dx, \tag{6}$$

where $A_{i,j}$ denotes the area of $\mathrm{SU}_{i,j}$. As an example, the OBCR calculation for Fig. 3 is calculated in the Appendix. Algorithm 2 summarizes the procedure for finding overlapping points of (5).

3.3. Optimization Formulation

In this work, we aim to maximize the probability of accurate sensing and OBCR to reduce energy consumption as possible. That is, the target system utilization to be maximized can be expressed as follows:

$$\sum_{i=1}^{N} \sum_{j=1}^{M} s_{i,j} \left\{ \alpha \Phi_{i,j}(\lambda_{i,j}) + \beta \Psi_{i,j} \right\}, \tag{7}$$

where α and β denote the weight factors, that is $\alpha + \beta = 1$ and $\alpha, \beta \in [0,1]$. In (7), we optimize the PU detection threshold, $\lambda_{i,j}$, with its minimum and maximum thresholds as λ_{min} and λ_{max}, respectively,

$$\lambda_{min} \le \lambda_{i,j} \le \lambda_{max}. \tag{8}$$

In addition, we optimize the beam decision binary indicator $s_{i,j}$. If beam $\mathrm{SU}_{i,j}$ is used for spectrum sensing, $s_{i,j}$ becomes 1; otherwise, it becomes 0. That is, all $s_{i,j}$ can be denoted as binary integer variables,

$$s_{i,j} \in \{0,1\}, \quad \forall i, j. \tag{9}$$

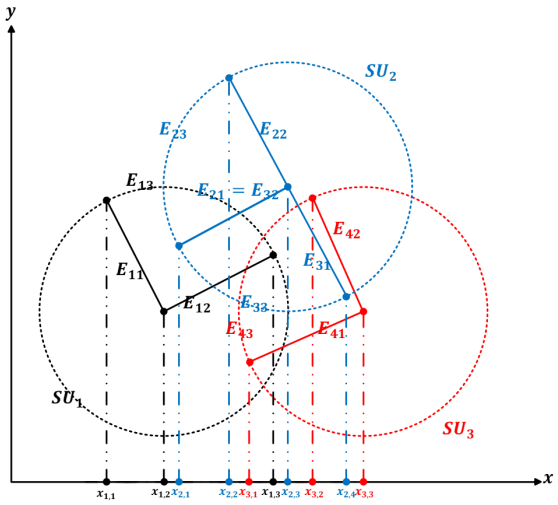

(a) Vertices of sectors.

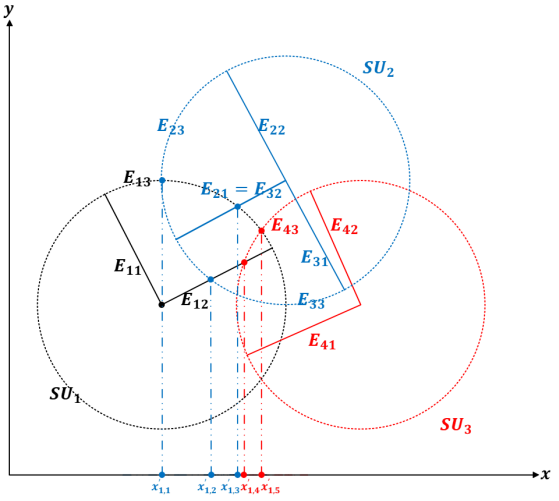

(b) Intersection points between sectors.

Figure 3: Example: vertices and intersection points between SU_{11} and other beams of SUs in the same LBZ.

Let $O_{i,j}$ denote an $N \times M$ sparse matrix with overlapping information, such that

$$O_{i,j}(n,m) = \left\{ \begin{array}{ll} 1, & \text{if } SU_{n,m} \text{ is overlapped with } SU_{i,j} \\ 0, & \text{otherwise} \end{array} \right\}.$$

That is, the matrix element $O_{i,j}(n,m)$ is 1 if beam $SU_{i,j}$ overlaps with beam $SU_{n,m}$. In this work, for energy-efficient beam sensing, for each beam $SU_{i,j}$, we switch on only one beam among overlapping neighboring beams. Therefore,

$$\sum_{n=1}^{N}\sum_{m=1}^{M} s_{n,m} O_{i,j}(n,m) = 1 \quad \forall i,j,. \tag{10}$$

Finally, the control variables $\lambda_{i,j}$ and $s_{i,j}$ can be expressed in the form of $N \times M$ matrices Λ and $\mathcal{S}$, respectively.

$$\Lambda = \begin{bmatrix} \lambda_{1,1} & \lambda_{1,2}, & \cdots & \lambda_{1,M-1}, & \lambda_{1,M} \\ \vdots & & \ddots & & \vdots \\ \lambda_{N,1} & \lambda_{N,2}, & \cdots & \lambda_{N,M-1}, & \lambda_{N,M} \end{bmatrix} \tag{11}$$

Algorithm 2 Finding Overlapping Points for LBZ_k

i, m: index of two distinct SUs in LBZ_k
j, n: index of beams of two distinct SUs
a, b: index of equation of two distinct beams
d: index of information of intersection point
k: index of LBZ
$E^i_{j,a}(x)$: equation if $a = 1$ then $L^i_{j,1}(x)$, else if $a = 2$ then $L^i_{j,2}(x)$, else if $a = 3$ then $R_{i,j}(x)$
for $i := 1$ **to** $|\,LBZ_k\,|$ **do**
  for $m := i + 1$ **to** $|\,LBZ_k\,|$ **do**
    if $\sqrt{|x_i - x_m|^2 + |y_i - y_m|^2} < r_i + r_m$ **then**
      $d \leftarrow 1$
      For all i, j, m, n of $SU_{i,j}$, $SU_{m,n}$,
      if $\exists x$ s.t. $|E^i_{j,a}(x) - E^m_{n,b}(x)| = 0$ **then**
        $p_d \leftarrow x$
        $q_{d-1} \leftarrow x$
        if $E^i_{p,a}(p_d + \epsilon) > E^j_{q,b}(p_d + \epsilon)$ **then**
          $E^U_d \leftarrow E^i_{j,a}(x)$
          $E^L_d \leftarrow E^m_{n,b}(x)$
        else
          $E^U_d \leftarrow E^j_{i,b}(x)$
          $E^L_d \leftarrow E^i_{j,a}(x)$
        end if
        $d \leftarrow d + 1$
      end if
    end if
    Sorting i_d in ascending order.
  end for
end for

$$\mathcal{S} = \begin{bmatrix} s_{1,1} & s_{1,2}, & \cdots & s_{1,M-1}, & s_{1,M} \\ \vdots & & \ddots & & \vdots \\ s_{N,1} & s_{N,2}, & \cdots & s_{N,M-1}, & s_{N,M} \end{bmatrix} \tag{12}$$

Therefore, the problem can be summarized as determining the optimal control variables $(\Lambda^*, \mathcal{S}^*)$ of the following problem:

$$\text{(P1)} \quad \max_{\Lambda,S} \quad (7) \quad \text{s.t} \quad (8), (9), (10). \tag{13}$$

4. Proposed Semi-Distributed Spectrum Sensing Control

In this work, we solve (P1) in a semi-distributed manner. To do so, we first decompose the problem (P1) into each LBZ_k basis local problem (P2), which can be solved, as in 4.1.

$$\text{(P2)} \quad \max_{\Lambda,S} \sum_{i \in LBZ_k} \sum_{j=1}^{M} s_{i,j} \left\{ \alpha \Phi_{i,j}(\lambda_{i,j}) + \beta \Psi_{i,j} \right\}, \tag{14}$$
$$\text{s.t} \quad (8), (9), (10).$$

Then, the leaders of the LBZ_k iteratively coordinate their solutions, as in Algorithm 4.

4.1. Concave Optimization with Elimination Approach

For each LBZ_k, the leader of the LBZ_k finds its local solution. In (14), $s_{i,j}$ is independent of $\Phi_{i,j}(\lambda_{i,j})$. Thus, the optimal

$s_{i,j}$ and $\lambda_{i,j}$ can be determined separately. First, to find optimal $\lambda_{i,j}$, we can check some properties of the function $\Phi_{i,j}(\lambda_{i,j})$. For simplicity, we use $\Phi(\lambda)$ rather than $\Phi_{i,j}(\lambda_{i,j})$ in the following propositions.

Proposition 1. *There exists an extreme point λ^* that satisfies the first derivative $\frac{\partial}{\partial x}\Phi(\lambda^*) = 0$.*

Proof. The function $\Phi_{i,j}(\lambda_{i,j})$ is a linear combination of the probability density functions (PDFs) of false alarm (P_{FA}) and missed detection ($1 - P_{CD}$), and therefore, it is continuous and differentiable. For convenience, let $x = \frac{\lambda}{2}$ for evaluating the derivative of $\frac{\Gamma(1,\frac{\lambda}{2})}{\Gamma(1)}$. As $\Gamma(u,x)$ is $\int_x^\infty t^{u-1}e^{-t}dt$, the first-order partial derivative of $\frac{\Gamma(1,x)}{\Gamma(1)}$ can be derived as follows:

$$\frac{\partial}{\partial x}\left(\frac{\Gamma(u,x)}{\Gamma(u)}\right)\Big|_{u=1} = -\exp(-x). \tag{15}$$

Subsequently, let $a = \sqrt{2\Upsilon}$ and $b = \sqrt{\lambda}$ to calculate the first-order partial derivative of the generalized momentum Q function $Q_1\left(\sqrt{2\Upsilon}, \sqrt{\lambda}\right)$ for convenience. Then, the first-order partial derivative of $Q_1(a,b)$ is derived based on [26] and [27] as follows:

$$\begin{aligned}
&\frac{\partial}{\partial b}Q_1(a,b)\\
&= \frac{\partial}{\partial b}\int_b^\infty x\exp\left(-\frac{a^2+x^2}{2}\right)I_0(ab)dx\\
&= (-b)\exp\left(-\frac{a^2+b^2}{2}\right)I_0(ab),
\end{aligned} \tag{16}$$

where I_n denotes the nth-order modified Bessel function in a series form. Therefore, the first-order partial derivative of Φ can be derived as follows:

$$\begin{aligned}
&\frac{\partial}{\partial\lambda}\Phi(\lambda)|_{u=1}\\
&= \exp\left(-\frac{\lambda}{2}\right) - \lambda^{\frac{1}{2}}\exp\left(-\frac{2\Upsilon+\lambda}{2}\right)I_0(\sqrt{2\Upsilon\lambda})\\
&= \exp\left(-\frac{\lambda}{2}\right)\cdot\left(1 - \sqrt{\lambda}\exp(-\Upsilon)I_0(\sqrt{2\Upsilon\lambda})\right).
\end{aligned} \tag{17}$$

The extreme point λ^* that equates (17) to zero with a constant Υ can be obtained through various numerical analysis methods. □

The function $\Phi(\lambda)$ also has the following property.

Proposition 2. *If λ^* is an extreme point, function $\Phi(\lambda)$ is concave if $\frac{\partial}{\partial\lambda}\Phi(\lambda^* - \epsilon) > 0$ and $\frac{\partial}{\partial\lambda}\Phi(\lambda^* + \epsilon) < 0$ for any $\epsilon > 0$.*

Proof. By substituting $\lambda^* + \epsilon$ into (17), we can derive the discriminant equation as follows:

$$\begin{aligned}
&\frac{\partial}{\partial\lambda}\Phi(\lambda)|_{u=1,\lambda=\lambda^*+\epsilon}\\
&= \exp\left(-\frac{\lambda^*+\epsilon}{2}\right) -\\
&\qquad (\lambda^*+\epsilon)^{\frac{1}{2}}\exp\left(-\frac{2\Upsilon+\lambda^*+\epsilon}{2}\right)I_0\left(\sqrt{2\Upsilon(\lambda^*+\epsilon)}\right)\\
&= \exp\left(-\frac{\epsilon}{2}\right)\left\{\exp\left(\frac{\lambda^*}{2}\right)\right.\\
&\qquad - {\lambda^*}^{\frac{1}{2}}\exp\left(-\frac{2\Upsilon+\lambda^*}{2}\right)I_0\left(\sqrt{2\Upsilon(\lambda^*+\epsilon)}\right)\\
&\qquad \left. - \epsilon^{\frac{1}{2}}\exp\left(-\frac{2\Upsilon+\lambda^*}{2}\right)I_0\left(\sqrt{2\Upsilon(\lambda^*+\epsilon)}\right)\right\},
\end{aligned} \tag{18}$$

where the first-order modified Bessel function I_0 is monotonically increasing in $(0,\infty)$. Therefore, if ϵ is a negligibly small positive value (but not zero), the first-order partial derivative of $\Phi(\lambda)$ is always negative. Similarly, if ϵ is an extremely small negative value (but not zero), the first-order partial derivative of $\Phi(\lambda)$ is always positive. Thus, $\Phi(\lambda)$ is concave, as illustrated in Fig. 4. □

Based on the Propositions 1 and 2, function $\Phi(\lambda)$ has the following property.

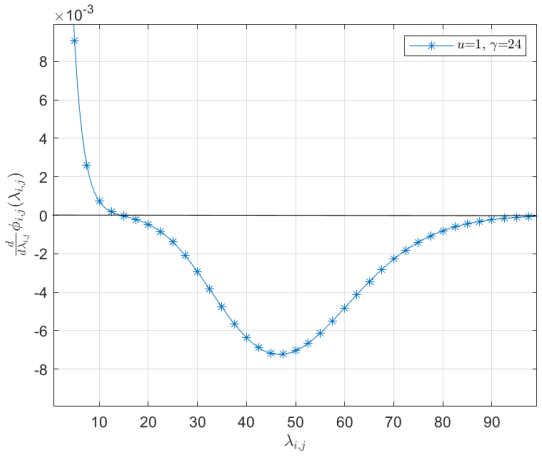

Figure 4: First derivative of $\Phi_{i,j}(\lambda_{i,j})$ with $u = 1$ and $\Upsilon_{i,j} = 24$.

Proposition 3. *Function $\Phi(\lambda)$ is quasi-concave for $\lambda \in (0,\infty)$.*

Proof. The first-order partial derivative is always positive if λ is less than λ^* and negative if it is greater than λ^*. In addition, based on the convergence properties of $\Gamma(1,\lambda)$ and $Q_1(\Upsilon_{i,j},\lambda)$, $\Phi(\lambda)$ converges if $\lambda \to \infty$. Therefore, the proposed accurate-sensing probability $\Phi(\lambda)$ is quasi-concave. □

Based on these properties, we can guarantee the existence and uniqueness of optimal $\lambda_{i,j}$ [28]. Therefore, we employed an gradient descent method to find the optimal $\lambda_{i,j}$ with modifying step size. With the optimal $\lambda_{i,j}$ (a constant variable), we use a modified elimination method to find the optimal $s_{i,j}$ in

(14) based on the constraint (10) for the overlapping information matrix $O_{i,j}$, as shown in Algorithm 3.

Algorithm 3 Modified Elimination Approach to Solve (P2)

1: **Input** : Problem (P2)
2: **Constraints** : (8), (9), (10)
3: **Solution Procedure** :
4: All $\mathrm{SU}_{i,j}$ are divided into sets of overlapping beams based on $O_{i,j}$.
5: Then, $s_{i,j}$ can be determined using (8) and (9) because only one beam will be turned on: the one that has the greatest value in each set (10).
6: The optimal solution is obtained by summing all derived $s_{i,j}$.
7: **Output** : Optimal Solution $\mathcal{S}^*$ of (P2)

4.2. Coordination between LBZs

The coordination process is shown in Algorithm 4. After local sensing of each LBZ, all LBZs broadcast its sensing information and connectivity table using LoRa (line 6). The distance between the SUs is checked for the channel that senses the same private sub-channel (PS) as the LBZ (line 12). At this time, if there is overlapping, the smaller beam, determined by comparing the OBCR, is turned off (line 13–17). After optimizing each LBZ, it is done in the stage of coordinating the optimization between LBZs, so it is almost closed as solving the problem of (P1).

4.3. Operational Flow and Computational Complexity

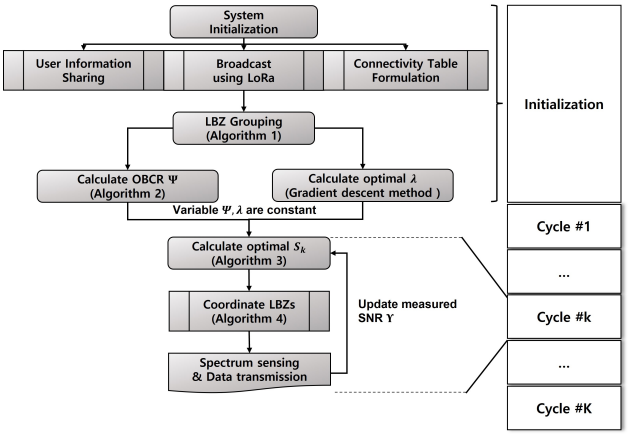

Figure 5: Proposed cooperative spectrum sensing timeline.

The overall spectrum sensing procedure can be summarized as in Fig. 5. For the complexity analysis below, recalling some symbols once again, N, K and M denote the number of SUs, the number of subchannels, and the number of beams per SU, respectively. In the initialize step, the main computational complexity for grouping LBZ (Algorithm 1) comes from formulation of connectivity table and calculation of OBCR Ψ. The

Algorithm 4 Localized Broadcast Zone Coordination

1: i, j : index of SU in connectivity table
2: m, n : index of beam
3: k, l : index of LBZ
4: $\hat{K}$: number of LBZs
5: **Step 1.** ***Sharing connectivity table between LBZs***
6: $\forall$ LBZ_k broadcast its sensing information and connectivity table using LoRa.
7: **Step 2.** ***Validation overlapping of beam direction***
8: **for** $k := 1$ to $\hat{K}$ **do**
9: **for** $l := k + 1$ to $\hat{K}$ **do**
10: **if** PS of LBZ_k == PS of LBZ_l **then**
11: **for** $i := 1$ to $|LBZ_k|$ **do**
12: Check for overlap with SU_j in LBZ_l based on $D(i, j) < R, \forall j$.
13: **if** $\forall m, n$, $\mathrm{SU}_{i,m}$ and $\mathrm{SU}_{j,n}$ are overlapped **then**
14: **if** $\Psi_{i,m} \geq \Psi_{j,n}$ **then**
15: $s_{i,m} \leftarrow 0$
16: **else**
17: $s_{j,m} \leftarrow 0$
18: **end if**
19: **end if**
20: **end for**
21: **end if**
22: **end for**
23: **end for**
24: **Step 3.** ***Update for next sensing and transmission***
25: Update and store the shared sensing information and connectivity table.
26: Shift PS for next cycle.

complexity becomes $O(N \log N)$. Finding optimal λ with gradient descent method has $O(N^2)$ computational complexity. Finding optimal S_k (Algorithm 3) employs a modified elimination approach, which is based on linear search and has $O(N^2)$ computational complexity. For LBZs coordination in Algorithm 4, the algorithm examines overlapswith different LBZs and adjusts overlapping beam to ON or OFF. This total sensing and transmission phase is repeated for each sub-channels, that is K times. Therefore, the overall computational complexity of the proposed algorithm becomes $O(KMN^2)$, which is polynomial complex. In addition, K and M can be generally assumed to be extremely small compared to N.

5. Performance Evaluation

In this section, we evaluate the performance of the proposed control in terms of spatial efficiency, detection accuracy, and energy consumption:

- Spatial Efficiency (%): This measures how efficiently spectrum sensing is carried out without beam overlapping for the entire sensing area.
- Sensing Accuracy (%): This measures the average accurate-sensing probability without false alarm and miss detection by SUs.

- Energy Consumption for Sensing (mJ): This measures the total energy consumption used for spectrum sensing by all SUs.

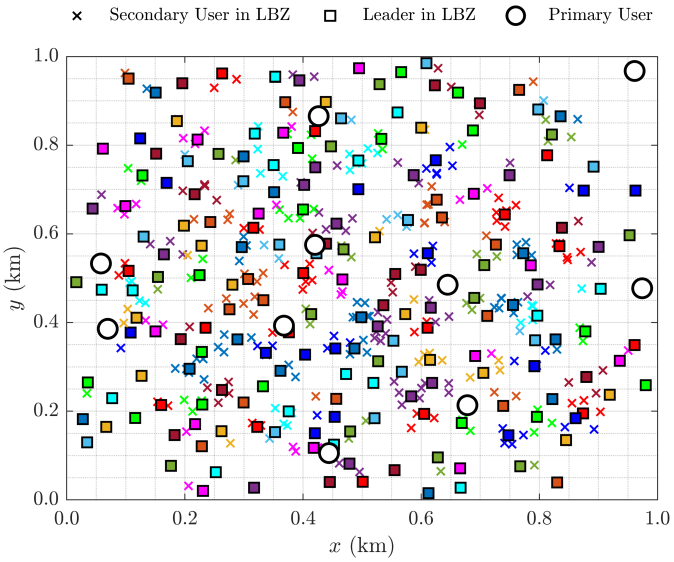

Figure 6: Simulation topology.

Table 3: Simulation Parameters

Parameter	**Value**
Topology Size	1 km × 1 km
Energy Consumption per Sensing	0.4 mJ
Bandwidth W	1 KHz
Sensing Period T_s	0.001 s
Number of Beams M	2 – 8
Number of PUs	10
Number of SUs N	100 – 2000
Sensing Distance of SU	0.1 – 0.5 km
Time-bandwidth Product u [**?**]	1

In this work, we compared the proposed control with following approaches:

- omnidirectional non-cooperative spectrum sensing: this method uses an omnidirectional antenna-based non-cooperative spectrum sensing model. It always turns on all beams and senses without considering overlapping sensing ranges.

- Directional centralized spectrum sensing [**?**]: This is a directional antenna-based centralized spectrum sensing scheme. The global FC collects the sensing information of all SUs and determines the optimal sensing beam of all the SUs.

- Directional fully distributed spectrum sensing [29]: This method is a directional antenna-based fully distributed sensing scheme. Unlike the proposed scheme, it does not employ any inter-LBZ coordination.

- Proposed sensing: This is the proposed directional antenna-based semi-distributed and cooperative spectrum sensing scheme.

For the evaluation, we implemented a simulator using the C and PYTHON programming languages and MATLAB optimization tool. In the simulation, the users were uniformly distributed over 1 km × 1 km regions, as shown in Fig. 6. The users were grouped into four LBZ, and each LBZ leader was selected. The simulation parameters were set as in Table 1.

Fig. 7 shows the correct-sensing probability $\phi_{i,j}$ according to the time-bandwidth product u and the measured SNR $\gamma_{i,j}$. In Fig. 7a and Fig. 7b, as u increases, $1 - P_{FA}$ increases more slowly, but P_{CD} is not affected. In contrast, as $\gamma_{i,j}$ increases, $1 - P_{FA}$ is not affected, but P_{CD} increases more slowly. On the other hand, because the correct-sensing probability $\phi_{i,j}$ is a linear combination of $1 - P_{FA}$ and P_{CD}, $\phi_{i,j}$ is affected by u and $\gamma_{i,j}$, as shown in Fig. 7c. As u increases, optimal $\lambda_{i,j}$ increases, and its $\phi_{i,j}$ value decreases. As $\gamma_{i,j}$ increases, optimal $\lambda_{i,j}$ and its $\phi_{i,j}$ value increases.

Fig. 8-11 compare the average system utilization, spatial efficiency, energy consumption, and detection accuracy for different numbers of SUs and measured SNRs, respectively. We conducted this simulation in an environment with $u = 1$ (sensing period $T_s = 0.001$ s and bandwidth W= 1KHz), which was used for the directional centralized cooperative spectrum sensing model [**?**].

Fig. 8 compared the average system utilization, where we set the performance of the omnidirectional sensing model to 100% as the baseline for comparison. In Fig. 8a, the system utilization of the all sensing approaches increases as the number of SUs increases. However, the performance of the directional antenna-based sensing models is superior to that of the omnidirectional sensing approach. The proposed model shows 33%−167% and 7%−12% better than the omnidirectional sensing and directional centralized sensing approaches, respectively, and 5$−8% worse than the directional centralized sensing approach. In Fig. 8b, there is almost no system utility change according to the measured SNR $\gamma_{i,j}$. The directional antenna-based sensing model were always superior to the omnidirectional sensing model under all the measured SNR $\gamma_{i,j}$. The proposed model provides 74% and 8% higher system utility than the omnidirectional sensing and directional fully distributed sensing approaches, respectively, and 7% lower system utility than the directional centralized sensing approach.

Fig. 9 shows the spatial efficiency. For the evaluation, we set the spatial efficiency of the omnidirectional sensing model to 100% as the baseline. Fig. 9a shows that the proposed model provided 31%−202% and 17%−97% better spatial efficiency than the omnidirectional sensing and directional fully distributed sensing approaches, respectively. This is because the proposed sensing model consider the sensing coverage overlapping, but the traditional omnidirectional model does not, and the directional fully distributed sensing model only considers sensing coverage overlap within a cluster. On the other hand, the proposed model provided 2%−7% lower spatial efficiency than the directional centralized approach. In Fig. 9b, there is almost no

spatial efficiency change according to $\gamma_{i,j}$. The proposed model provides 66% and 36% higher spatial efficiency than the omnidirectional sensing and directional fully distributed sensing approaches, respectively, and 4% lower spatial efficiency than the directional centralized sensing approach.

Fig. 10 shows energy consumption. In Fig. 10a, when the number of SUs is 500, the proposed semi-distributed model showed 25% and 16% less energy than the omnidirectional sensing and directional fully distributed sensing approaches, respectively. As the number of SUs up to 2,000, its energy-saving gains increased to 67% and 50%, respectively. This is because the number of sensing beams overlapping between SUs or LBZs increase as the number of SUs increases. Therefore, the performance gap gradually increases as the number of SUs increases. The proposed approach consumed slightly more energy than the directional centralized approach, but its difference is within 1%. In Fig. 10b, the energy consumption of the comparative models was fixed regardless of $\gamma_{i,j}$. However, the energy consumption with the proposed model changed slightly as $\gamma_{i,j}$ changed. This is because, unlike the comparative models, the proposed model considers its energy consumption when determining the optimal beam strategy. The proposed sensing model consumed approximately 41% and 27% less energy than the omnidirectional sensing model and directional full distributed sensing model. On the other hand, the proposed approach consumed approximately 4% more energy than the directional centralized approach.

Fig. 11 shows the average sensing accuracy. In Fig. 11a, for all cases where the user number is different, the proposed model is slightly more accurate than the omnidirectional sensing and directional fully distributed sensing approaches, and it is slightly less accurate than the directional centralized sensing approach. However, all the schemes, including the proposed scheme, provided very high accuracy, above 98.4%. On the other hand, in Fig. 11b, all schemes provide almost same sensing accuracy, and the sensing accuracy contiued to increase to nearly 100% as the γ increases. This is because it becomes easier to determine whether the sensed signal is a licensed spectrum signal or noise as the measured SNR increases. That is, this result shows that the proposed approach provides very high sensing accuracy with significantly reduced energy consumption.

6. Conclusion

In this paper, as an alternative to centralized spectrum sensing approaches, we proposed a directional antenna-based semi-distributed and cooperative passive spectrum sensing scheme. As a solution framework, we translated the centralized spectrum sensing problem to distributed spectrum sensing problem with a modified elimination method and coordination method between LBZs. We proved the concavity of the formulated problem with perspective of λ and found optimal λ with descent gradient method. Then, we found the optimal beam ON/OFF solution $\mathcal{S}$ by a modified elimination method. We also proposed a low-complex coordination mechanism among LBZ leaders for efficient spectrum sensing and close to original centralized spectrum sensing problem. A simulation confirmed that the proposed scheme is superior to the existing omnidirectional antenna-based sensing and directional antenna-based fully distributed sensing approaches in terms of sensing accuracy, spatial efficiency, sensing energy consumption. The performance gain increases as the number of SUs increases. It is also confirmed that the proposed scheme achieves a near-optimal performance within around 5% of a directional antenna based centralized spectrum sensing approach. The experimental can be efficiently applied to directional antenna-based cognitive IoT networks.

Appendix A. Example of OBCR Calculation

In Fig. 3, SU_1 overlaps two beams of SU_2 and one beam of SU_3. Then, the OBCRs between SU_1, SU_2, and SU_3 are illustrated in Fig. 12. Therefore, $\Psi_{1,1}$ can be evaluated as in (A.1).

$$
\begin{aligned}
\Psi_{1,1} &= \frac{1}{A_{i,j}} \sum_{n=1}^{3} \sum_{d=1}^{|I_{1,n}^{k,1}|} \int_{p_d}^{p_{d+1}} \left\{ E_d^U(x) - E_d^L(x) \right\} dx \\
&= \frac{1}{A_{i,j}} \Big[\int_{x_{1,1}^{'}}^{x_{2,1}} \{E_{13}(x) - E_{23}(x)\} dx + \\
&\qquad \int_{x_{2,1}}^{x_{1,2}^{'}} \{E_{21}(x) - E_{13}(x)\} dx + \\
&\qquad \int_{x_{2,1}}^{x_{1,2}^{'}} \{E_{32}(x) - E_{33}(x)\} dx + \\
&\qquad \int_{x_{1,2}^{'}}^{x_{1,3}^{'}} \{E_{13}(x) - E_{33}x)\} dx + \\
&\qquad \int_{x_{1,3}^{'}}^{x_{1,3}} \{E_{13}(x) - E_{12}(x)\} dx + \\
&\qquad \int_{x_{1,4}^{'}}^{x_{1,5}^{'}} \{E_{43}(x) - E_{12}(x)\} dx + \\
&\qquad \int_{x_{1,5}^{'}}^{x_{1,3}} \{E_{13}(x) - E_{12}x)\} dx \Big].
\end{aligned}
\tag{A.1}
$$

References

[1] M. S. Gupta, K. Kumar, Progression on spectrum sensing for cognitive radio networks: A survey, classification, challenges and future research issues, Journal of Network and Computer Applications 143 (2021) 47–74. doi:10.1016/j.jnca.2019.06.005.

[2] I. F. Akyldiz, B. F. Lo, R. Balakrishnan, Cooperative spectrum sensing in cognitive radio networks: A survey, Physical Communication 4 (2011) 40–62. doi:10.1016/j.phycom.2010.12.003.

[3] R. Wan, M. Wu, L. Hu, H. Wang, Energy-efficient cooperative spectrum sensing scheme based on spatial correlation for cognitive Internet of Things, IEEE Access 8 (2020) 139501–139511. doi:10.1109/ACCESS.2020.3010989.

[4] A. Paul, A. Daniel, A. Ahmad, S. Rho, Cooperative cognitive intelligence for internet of vehicles, IEEE Systems Journal 11 (3) (2017) 1249–1258. doi:10.1109/JSYST.2015.2411856.

[5] K. Wu, H. Jiang, C. Tellambura, Cooperative sensing with heterogeneous spectrum availability in cognitive radio, IEEE Transactions on Cognitive Communications and Networking 8 (1) (2022) 31–46. doi:10.1109/TCCN.2021.3085769.

[6] P. Amirshahi, P. Ransom, S. Grippando, I. Navarro, Comparison of centralized and distributed spectrum monitoring methods for enabling spectrum sharing between weather satellites and terrestrial networks, 2019 IEEE International Symposium on Dynamic Spectrum Access Networks (DySPAN) (2019) 1–8doi:10.1109/DySPAN.2019.8935816.

[7] Z. Wei, B. Zhao, J. Su, Cooperative sensing in cognitive radio ad hoc networks, 2019 IEEE International Conference on Communications (ICC) (2019) 1–6doi:10.1109/ICC.2019.8761461.

[8] A. H. Gazestani, S. A. Ghorashi, Distributed diffusion-based spectrum sensing for cognitive radio sensor networks considering link failure, IEEE Sensors Journal 18 (20) (2018) 8617–8625. doi:10.1109/JSEN.2018.2866429.

[9] P. J. Smith, R. Senanayake, P. A. Dmochowski, J. S. Evans, Distributed spectrum sensing for cognitive radio networks based on the sphericity test, IEEE Transactions on Communications 67 (3) (2019) 1831–1844. doi:10.1109/TCOMM.2018.2880902.

[10] Z. Gu, Y. Wang, T. Shen, F. C. M. Lau, On heterogeneous sensing capability for distributed rendezvous in cognitive radio networks, IEEE Transactions on Mobile Computing 20 (11) (2021) 3211–3226. doi:10.1109/TMC.2020.2997077.

[11] W. U. Mondal, A. A. Sardar, N. Biswas, G. Das, Nash bargaining-based economic analysis of opportunistic cognitive cellular networks, IEEE Transactions on Cognitive Communications and Networking 6 (1) (2020) 242–255. doi:10.1109/TCCN.2019.2948325.

[12] B. Ning, G. Sun, J. Li, A. Zhang, W. Hao, S. Yang, Resource allocation in multi-user cognitive radio network with stackelberg game, IEEE Access 8 (2020) 58260–58270. doi:10.1109/ACCESS.2020.2981556.

[13] Digital Video Broadcasting (DVB), Tech. Rep. EN 300 744, V1.6.2, ETSI Standard (2015).

[14] C. L. Wang, H. W. Chen, A new signal structure for active sensing in cognitive radio systems, IEEE Transactions on Communications 62 (3) (2014) 822–835. doi:10.1109/TCOMM.2014.011614.120732.

[15] A. A. Abdullah, L. Cai, F. Gebali, DSDMAC: dual sensing directional MAC protocol for Ad Hoc networks with directional antennas, IEEE Transactions on Vehicular Technology 61 (3) (2012) 1266–1275. doi:10.1109/TVT.2012.2187082.

[16] D. L. Wasden, H. Moradi, , B. Farhang-Boroujeny, Design and implementation of an underlay control channel for cognitive radios, IEEE Journal on Selected Areas in Communications 30 (10) (2012) 1875–1889. doi:10.1109/JSAC.2012.121104.

[17] H. Lei, C. Gao, I. S. Ansari, Y. Guo, Y. Zou, G. Pan, K. A. Qaraqe, Secrecy outage performance of transmit antenna selection for MIMO underlay cognitive radio systems over Nakagami-m channels, IEEE Transactions on Vehicular Technology 66 (3) (2017) 2237–2250. doi:10.1109/TVT.2016.2574315.

[18] Q. Huang, Z. Luo, J. Zhang, W. Wang, Q. Zhang, LoRadar: Enabling concurrent radar sensing and LoRa communication, IEEE Transactions on Mobile Computing (2020 [Online]. doi:10.1109/TMC.2020.3035797).

[19] L. Li, Y. Qin, X. Zhong, A novel routing scheme for resource-constraint opportunistic networks: A cooperative multiplayer bargaining game approach, IEEE Transactions on Vehicular Technology 65 (8) (2016) 6547–6561. doi:10.1109/TVT.2015.2476703.

[20] W. Na, L. Park, S. Cho, Deafness-aware mac protocol for directional antennas in wireless ad hoc networks, Elsevier Ad Hoc Networks Journal 24 (2015) 121–134. doi:10.1016/j.adhoc.2014.08.005.

[21] R. C. Qiu, Z. Hu, H. Li, M. C. Wicks, Cognitive radio communications and networking : principles and practice, Oxford:Wiley, 2012.

[22] N. A. R.-Smith, K. Humood, An Efficient Scheme in IEEE 802.22 WRAN for Real Time and Non Real Time Traffic Delay, LAP LAMBERT Academic, 2012.

[23] S. Song, K. Letaief, Spectrum sensing with active cognitive systems, IEEE Transactions on Wireless Communications 9 (6) (2010) 1849–1854. doi:10.1109/TWC.2010.06.090924.

[24] F. F. Digham, M. S. Alouini, M. K. Simon, On the energy detection of unknown signals over fading channels, IEEE Transactions on Communications 55 (1) (2007) 21–24. doi:10.1109/TCOMM.2006.887483.

[25] Y. Sun, A. Baricz, S. Zhou, On the monotonicity, log-concavity, and tight bounds of the generalized Marcum and Nuttall Q-functions, IEEE Transactions on Information Theory 56 (3) (2010) 1161–1186. doi:10.1109/TIT.2009.2039048.

[26] W. Pratt, Partial differentials of Marcum's Q function, Proceedings of the IEEE 56 (7) (1968) 1220–1221. doi:10.1109/PROC.1968.6526.

[27] R. Esposito, Comment on "partial differentials of marcum's q function", Proceedings of the IEEE 56 (12) (1968) 2195–2195. doi:10.1109/PROC.1968.6856.

[28] C. Ozturk, B. Dulek, S. Gezici, Convexity properties of detection probability for noncoherent detection of a modulated sinusoidal carrier, IEEE Transactions on Vehicular Technology 67 (12) (2018) 12410–12415. doi:10.1109/TVT.2018.2876516.

[29] Y. Chen, S. Su, H. Yin, X. Guo, Z. Zuo, J. Wei, L. Zhang, Optimized non-cooperative spectrum sensing algorithm in cognitive wireless sensor networks, Sensors 19 (9) (2019). doi:10.3390/s19092174.

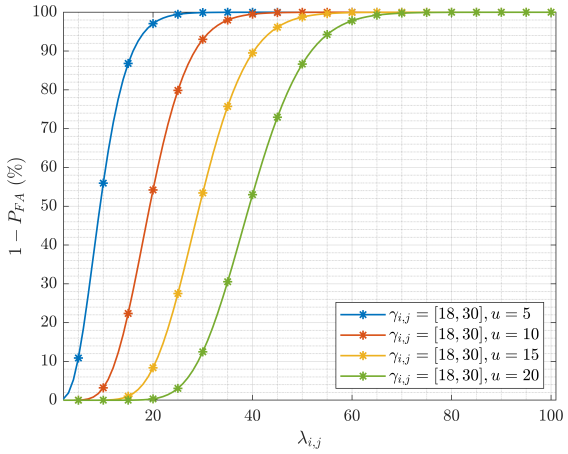

(a) $1 - P_{FA}$ vs. $\lambda_{i,j}$.

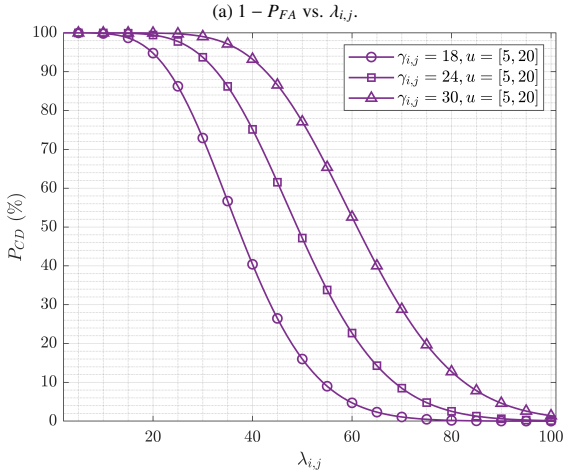

(b) P_{CD} vs. $\lambda_{i,j}$.

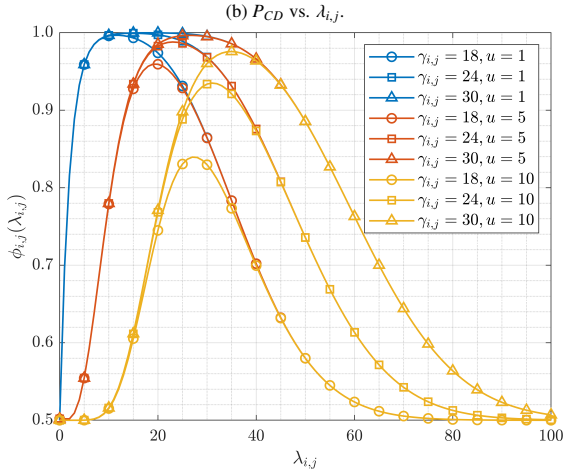

(c) Probability of accurate-sensing vs. $\lambda_{i,j}$.

Figure 7: Impact of u, and $\gamma_{i,j}$ on accurate-sensing probability.

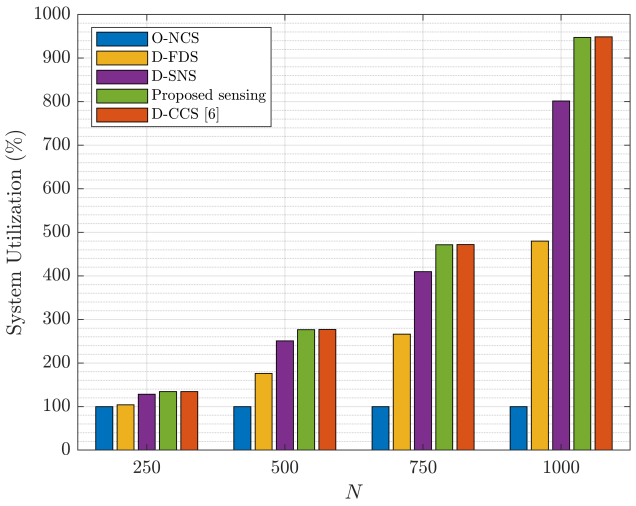

(a) Average system utilization with $\gamma_{i,j}$ = 24.

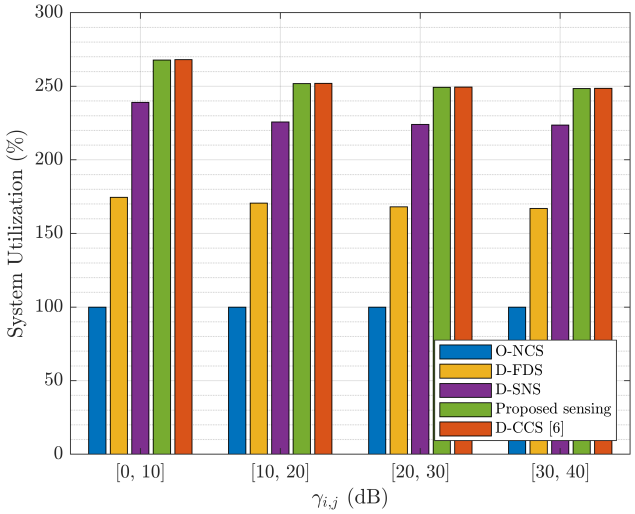

(b) Average system utilization with N = 1000.

Figure 8: Comparison of average system utilization vs. the number of SUs N and the estimated SNR $\gamma_{i,j}$.

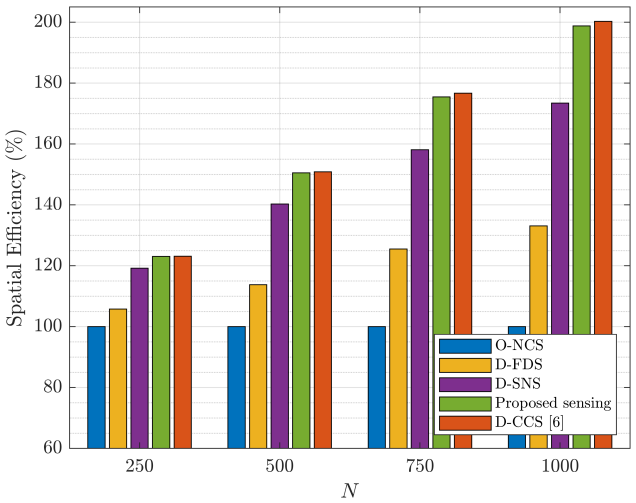

(a) Spatial efficiency with $\gamma_{i,j}$ = 24.

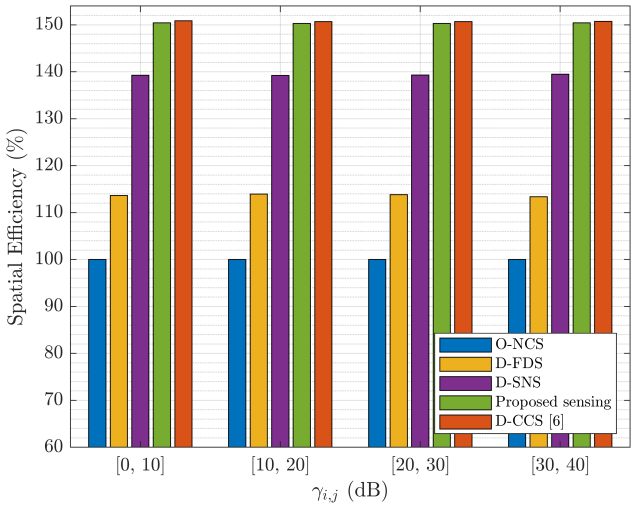

(b) Spatial efficiency with N = 1000.

Figure 9: Comparison of spatial efficiency vs. number of SUs N and the estimated SNR $\gamma_{i,j}$.

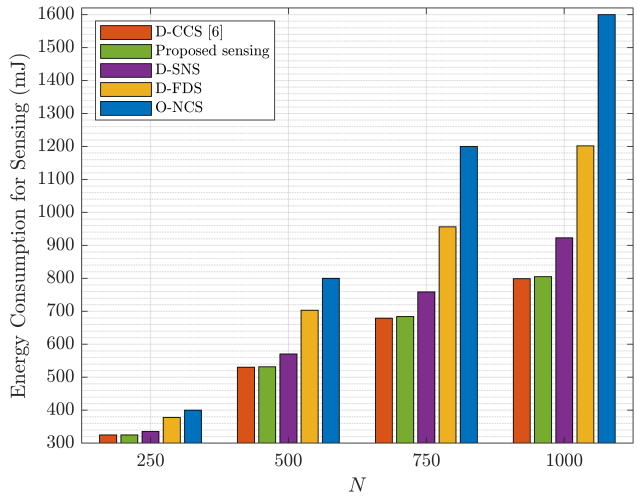

(a) Energy consumption with $\gamma_{i,j}$ = 24.

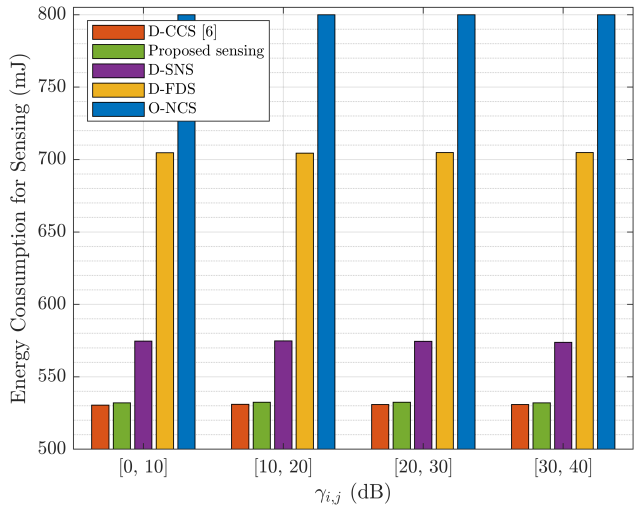

(b) Energy consumption with N = 1000.

Figure 10: Comparison of Energy consumption vs. the number of SUs N and the estimated SNR $\gamma_{i,j}$.

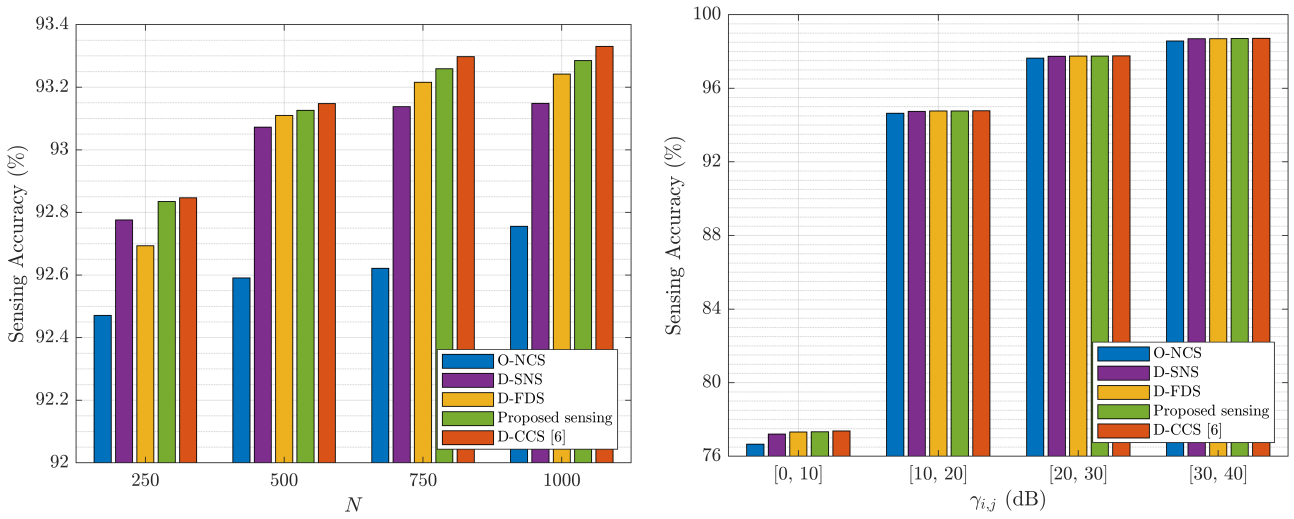

(a) Sensing accuracy with $\gamma_{i,j} = 24$.

(b) Sensing accuracy with $N = 1000$.

Figure 11: Comparison of sensing accuracy vs. the number of SUs N and the estimated SNR $\gamma_{i,j}$.

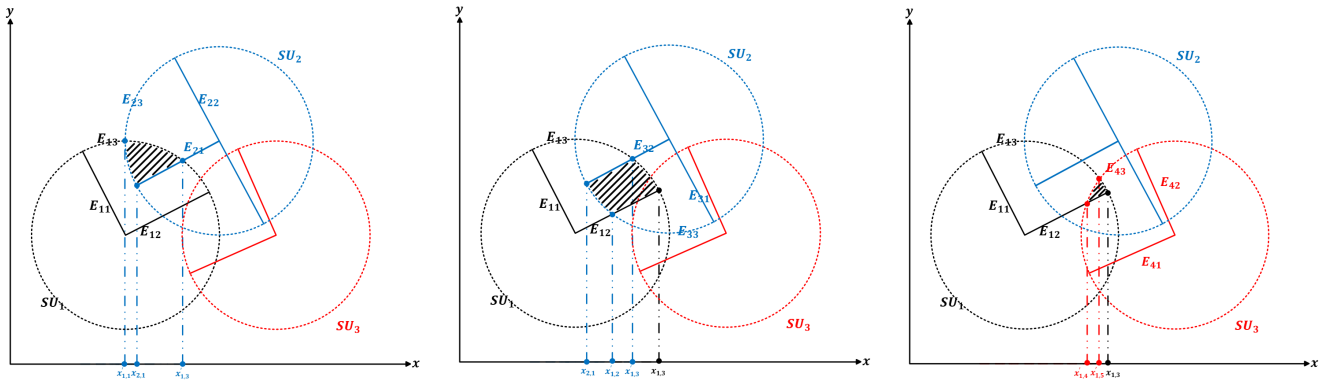

(a) Overlapping beam coverage ratio between SU_{11} and beam 2 of SU_{22}.

(b) Overlapping beam coverage ratio between SU_{11} and SU_{23}.

(c) Overlapping beam coverage ratio between SU_{11} and SU_{34}.

Figure 12: Example: calculation of overlapping beam coverage ratio $\Psi_{1,1}$.